

RemNet: Remnant Convolutional Neural Network for Camera Model Identification

Abdul Muntakim Rafi, Thamidul Islam Tonmoy, Uday Kamal, Rakibul Hoque, and Md. Kamrul Hasan*

Abstract—Camera model identification has gained significant importance in image forensics as digitally altered images are becoming increasingly commonplace. In this paper, we present a solution to the problem of identifying the source camera model of an image using a novel deep learning architecture called Remnant Convolutional Neural Network (RemNet). RemNet is comprised of multiple remnant blocks with intra-block skip connection and a classification block in series. Unlike the conventional fixed filters used in image forensics for preprocessing, our proposed novel remnant blocks are completely data driven. It suppresses unnecessary image contents dynamically and generates a remnant of the image from where the classification block can extract intrinsic camera model-specific features for model identification. The whole architecture is trained end-to-end. This network proves to be very robust for identifying the source camera model, even if the original images are post-processed. The network, trained and tested on 18 models from Dresden database, shows 100% accuracy for 16 camera models with an overall accuracy of 97.59% where the test dataset consisted of images from unseen devices. This result is better in comparison to other state of the art methods. Our network also achieves an overall accuracy of 95.01% on the IEEE Signal Processing (SP) Cup 2018 dataset, which indicates the generalizability of our network. In addition, RemNet achieves an overall accuracy of 99.53% in image manipulation detection which implies that it can be used as a general purpose network for image forensic tasks.

Index Terms—Image Forensics, Camera Model Identification, Convolutional Neural Networks, Remnant Blocks, Image Manipulation

I. INTRODUCTION

CAMERA model identification (CMI) is an important topic in image forensics and has applications in crucial tasks such as criminal investigations, authenticating evidence, detecting forgery, etc. This topic has gained even more relevance in recent years as digitally altered images are becoming more pervasive in electronic media. Now-a-days, professional image editing tools are readily available, thus, making image forgery quite commonplace. Although, some information about the source of an image can be obtained from metadata, this data can be forged as well. Since none of these image-markers can be considered as a reliable metric to determine the source, the task of identifying the camera model becomes very challenging. As a result, a forensic analyst has to resort to image processing techniques to identify the camera model with which an image was taken.

A number of methods have been proposed in the literature to perform this task. An extensive review of these methods can

be found in [1], [2]. Initially, researchers have tried to merge external features, e.g., watermarks, device-specific-code, etc., present in an image for the purpose of device identification [3]. However, adding different extrinsic features to every single camera being used has proved to be an unmanageable task [4]. As a result, focus has shifted towards detecting intrinsic camera features, such as the Color Filter Array (CFA) pattern [5], interpolation algorithms and Image Quality Metrics (IQM) used in the camera [6], [7]. Device-specific camera detection schemes have also been proposed, where noise patterns like the Photo Response Non-Uniformity (PRNU) have been exploited to identify the device [8]–[10]. Although device specificity is an inherent feature of PRNU noise, forensic researchers have developed methods to make camera model identification device invariant [11], [12]. Most of these try to estimate the model-specific artifacts that are introduced into an image during image capture and then correlate these features with a reference for the corresponding camera model [13]. In this approach, the second order statistics of the CFA pattern [14] and 3D co-occurrence matrices [15], [16] have been used as feature vectors to successfully detect camera models with state-of-the-art accuracy.

Most of the methods stated so far have used traditional complex ensemble classifiers. Recently, researchers have adopted a data-driven approach and made an effort to solve CMI problem using Convolutional Neural Networks (CNNs). This suggestion seems quite promising because, of late, CNNs have achieved phenomenal accuracy on image classification benchmarks [17]. Usually CNNs tend to learn features related to the contents of an image, whereas in CMI, we need to refrain CNNs from learning image contents associated with the camera models. As a result, a common practice while using CNNs in digital image forensics is adding a preprocessing layer at the beginning of the CNN architecture. Chen et. al [18] have proposed using a median filter whereas Tuama et al. [19] have used a high-pass filter before feeding images in their respective CNNs. Bayar et al. [20] have proposed a data-driven constrained convolutional layer which is superior in performance to both median and high pass filters. In [21], a concept of Fusion Residual Network (FRN) is proposed which uses the idea of using multi-scale receptive fields on an input image. It extracts intrinsic features from the input image by applying convolutions with different kernel size and then concatenates the feature maps. Seeing the improvement of results associated with the different preprocessing schemes, it has become evidently clear that the a customized preprocessing operation should be explored thoroughly in this field.

Also, in spite of the breadth of works performed in this

All authors are with the Department of Electrical and Electronic Engineering, Bangladesh University of Engineering and Technology, Dhaka-1205, Bangladesh.

E-mail: *khasan@eee.buet.ac.bd

field, little attention has been given to the identification of camera models from images of unseen devices. In addition, the performance of existing CMI methods on post-processed images, e.g., JPEG compressed, resized, gamma-corrected, etc., is not well studied. Although some researchers have explored the case of detecting image manipulation discretely [20], [22]–[25], not many have tried to bring them to the same framework. In reality, a robust CMI network needs to correctly predict the source camera model of an image which may have gone through diverse *post-processing* and captured from a previously *unseen* device.

In this paper, we propose a novel CNN architecture, called Remnant Convolutional Neural Network (RemNet), for identifying camera models from extensively post-processed images acquired with unseen devices. The network is comprised of two parts– a preprocessing block consisting of several remnant blocks with intra-block skip connections and a classification block. Remnant blocks constitute the core architecture of our network. It suppresses the unnecessary contents of the input image dynamically and outputs a remnant of the image from where high level camera model-specific features can be extracted. This is achieved through the use of several convolution layers with skip connections in between. We omit the activation function so as to make it perform a linear filter. The remnant blocks are followed by a classification block which learns higher-level discriminative features utilizing the useful information provided by the remnant blocks. However, the problem of overfitting still remains since existing datasets are limited in their sizes. To overcome this setback and to ensure generalization of the features that are learned, we use a number of data-augmentation schemes such as gamma-correction, JPEG compression, re-scaling. Our training procedure helps the network learn more robust camera model-specific features.

The rest of the paper is organized as follows. Section II provides a brief overview on CNNs. Section III presents a detailed description of our proposed architecture along with the motivations and intuitions behind designing it. Section IV provides a thorough discussion of the training and evaluation procedure along with the experimental results obtained after testing the model with different datasets on different image forensic tasks. Finally, we conclude in Section V.

II. CONVOLUTIONAL NEURAL NETWORKS

Convolutional neural networks are particular types of deep neural networks that have gained attention from research community and industry, achieving empirical successes in tasks such as object recognition, object detection, speech recognition, and natural language processing [26]. They automatically extract discriminative features from raw input information which are very difficult to obtain through traditional hand-crafted feature engineering [26].

In a typical CNN, the input information is passed through several convolution layers where they are convolved with the filters to generate output feature maps. If x_m^l is the m -th input

feature in the l -th layer, then the n -th output feature in that layer y_n^l is computed as

$$y_n^l = \sum_m^{M^{l-1}} w_{n,m}^l * x_m^l + b_n^l, \quad (1)$$

where M^{l-1} is the number of input maps, $*$ denotes convolution operation, and b_n^l is the bias of the n -th output map in the l -th level.

The convolution operations are usually followed by activation functions. The purpose of these functions are to introduce nonlinearity in the network. In computer vision tasks, ReLU [27] is the most popular choice for activation which is defined as

$$f(y_i) = \begin{cases} y_i, & \text{if } y_i > 0 \\ 0, & \text{if } y_i \leq 0 \end{cases} \quad (2)$$

However, ReLU activation applies a constraint on feature generation by passing only positive values while all negative values are set to zero. As a result, a number of modifications of the ReLU function have been proposed in the literature of which Parametric ReLU (PReLU) [28] has gained popularity in image recognition tasks in recent years. Instead of setting the negative values to zero, PReLU incorporates a learnable parameter a_i as

$$f(y_i) = \begin{cases} y_i, & \text{if } y_i > 0 \\ a_i y_i, & \text{if } y_i \leq 0 \end{cases} \quad (3)$$

While training neural networks, internal covariance shift causes the distribution of each layer’s inputs to change which subsequently slows down the training process. To mitigate this problem, researchers have proposed various normalizing schemes of which batch normalization (BN) [29] is used extensively in recent works. If x_i is the i -th input feature in a mini-batch \mathcal{B} with m input features, then the output y_i with BN is calculated as

$$\mu_{\mathcal{B}} = \frac{1}{m} \sum_{i=1}^m x_i, \quad (4)$$

$$\sigma_{\mathcal{B}}^2 = \frac{1}{m} \sum_{i=1}^m (x_i - \mu_{\mathcal{B}})^2, \quad (5)$$

$$\hat{x}_i = \frac{x_i - \mu_{\mathcal{B}}}{\sqrt{\sigma_{\mathcal{B}}^2 + \epsilon}}, \quad (6)$$

$$y_i = \gamma \hat{x}_i + \beta, \quad (7)$$

where $\mu_{\mathcal{B}}$ and $\sigma_{\mathcal{B}}^2$ are the mean and the variance of the mini-batch, respectively, and β and γ are two learnable parameters.

To reduce the dimensionality of the feature maps, various pooling operations are performed, such as, max-pooling, average-pooling, etc. The max-pooling operation takes a window of $q \times q$ and keeps only the maximum value of the selected window whereas average-pooling keeps only the average value. Pooling layers perform subsampling on the feature space in such a way that the most dominant features are retained.

The input is passed through successive convolutional layers along with activation, BN and pooling layers. Eventually, the feature space is gradually reduced to the number of classes

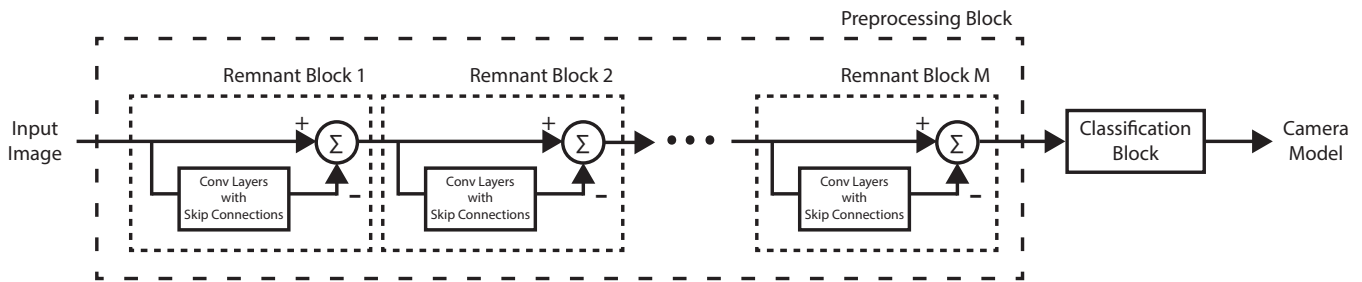


Fig. 1. Block diagram of our proposed method.

N to get $y = [y_1, y_2, \dots, y_N]$, where y_i represents the score of the i -th class. Finally, a softmax activation is applied on the output layer mapping the N class scores to N probability values $p = [p_1, p_2, \dots, p_N]$ for each class which sum up to 1:

$$p_i = \frac{\exp(y_i)}{\sum_{n=1}^N \exp(y_n)}. \quad (8)$$

The training of a neural network is conducted through successive forward and backward propagations of the data. During each forward pass, we get a probability output score for each input data. A loss is then calculated based on the predicted output and the ground truth. For multi-class classification problems, categorical crossentropy loss function is mostly used which is given by

$$L = \sum_{k=1}^N y_i^{*(k)} \log(y_i^{(k)}), \quad (9)$$

where $y_i^{*(k)}$ and $y_i^{(k)}$ are, respectively, the true label and the network output of the i -th image at the k -th class among the N classes. This loss is backpropagated to update the weights of the network parameters by using various optimization algorithms, such as, stochastic gradient descent (SGD) [30] and adaptive momentum (Adam) [31].

III. PROPOSED METHOD

We propose here a novel CNN based architecture for CMI. A data-driven preprocessing block is used at the beginning of the network which is followed by a classification block (see Fig. 1). The details of the proposed RemNet are presented in the following.

A. Motivation

To explain the motivation of our proposed method, we first describe the image acquisition pipeline of digital cameras depicted in Fig. 2. In a typical digital camera, the light of

a scene passes through a system of lenses and optical filters, which is then collected by an optical sensor. A colour filter array (CFA) is used before the sensor to obtain RGB colour images so that individual sensor element records light of a certain color. The remaining colour information is estimated from surrounding pixels through a process called CFA interpolation or demosaicing. After demosaicing, the image goes through a number of post-processing (e.g., color correction, edge enhancement, and compression) before it is saved on a storage device. As described in [2], most of these components leave certain ‘fingerprints’ in the image which can be utilized in different image forensic tasks. Manufacturers generally employ different lens systems in their different camera models which causes lens distortion artifacts, such as, radial lens distortion, chromatic aberration and vignetting. The CFA layout and demosaicing process vary widely among different models and are generally considered as one of the most distinctive model-specific signatures. The sensor pattern noise (SPN) is the most unique characteristic of a digital camera and it is used excessively in the literature for source identification.

In designing CNNs for image forensic tasks, it has been therefore a common practice to use a pre-processing scheme to suppress the image contents and intensify the minute signatures induced by the image acquisition pipeline. This is because, CNNs, in their standard form, tend to learn content-specific features from the image. To this end, different authors have employed different preprocessing schemes before training their CNNs. Chen et al. [18] fed their CNN with the median filtered residue of the images. Tuama et al. [19] used a fixed high-pass filter on the input image before feeding the data to a CNN. However, the reason behind using specific kernel coefficients or a particular kernel size is not well explained in [18], [19]. The shortcoming with these approaches are that human intervention is needed in designing the filters and, most importantly, these filters may not generalize on different datasets. Also, as mentioned in [12], the signatures left by different components in the image acquisition pipeline have

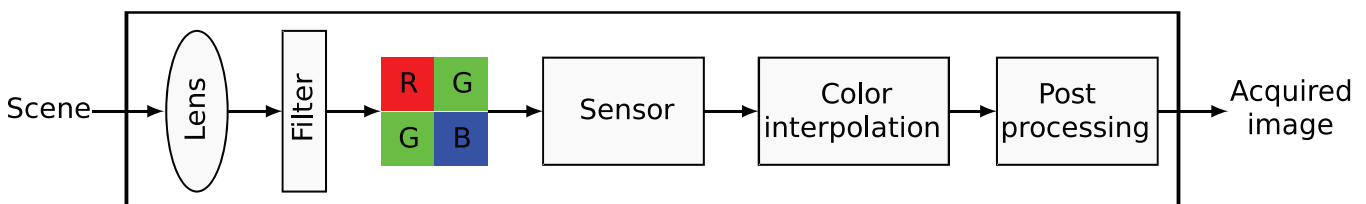


Fig. 2. General image acquisition pipeline of digital cameras.

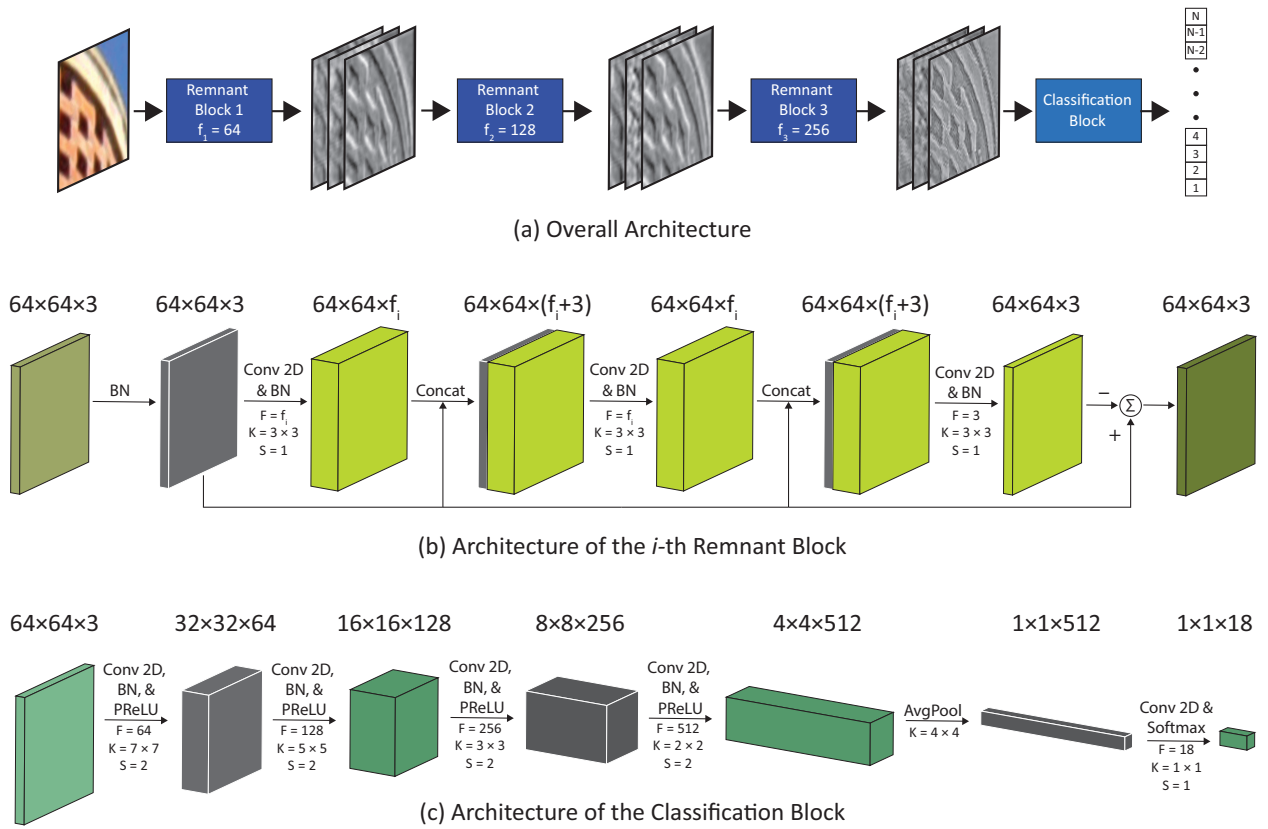


Fig. 3. Architecture of our proposed RemNet. (a) Illustrates the overall architecture with three remnant block with one classification block. The architectures of the remnant and classification blocks are depicted in (b) and (c), respectively. In (b) and (c), AvgPool, BN, and Conv2D represents average pooling, batch normalization and 2D convolution, respectively. The letters F, K, and S represent the number of filters, their kernel size, and strides, respectively, in the corresponding convolution layers.

different frequency ranges— demosaicing and vignetting leave low-frequency patterns whereas the SPN introduces high-frequency components. Since there are some camera model-specific features in the low-frequency range, using a high-pass filter may result in loss a of valuable camera model-specific features. A specific kernel size for median filtering may not also serve the purpose optimally.

To overcome the difficulties associated with designing an optimum filter for preprocessing, a data adaptive constrained convolutional layer is introduced by Bayar et al. [20]. The proposed preprocessing method in [20] extracts prediction error features from the image. However, the constrained convolution was first proposed for image manipulation detection [25] and it is not well explained how prediction error features retain camera model-specific features.

Therefore, our main goal is to introduce a preprocessing scheme that is completely data-driven but without any imposed constraints. This strategy is proven to be crucial for extraction of superior camera model-specific higher level features for our classification task as evident from our experimental results (Section IV). The benefit of designing such a preprocessing block is that it can dynamically adapt itself to perform different image forensic tasks.

B. Network Architecture

In this paper, we propose a novel CNN based architecture, RemNet, to identify camera model of an image. Our

architecture comprises of two parts— remnant blocks and a classification block. The remnant block is a data driven custom preprocessing scheme on the input image that suppresses image contents to some extent as required and intensifies camera model-specific feature-rich portions of the image at its output. The classification block attempts to generate a prediction based on the output of the final remnant block.

1) *Remnant block*: The camera model-specific features inherent in an image are very subtle and minute features of the image [1], [12], [32]. Detecting these features are difficult in itself and the task is made even more challenging because of the existence of device-specific features such as Photo Response Non Uniformity (PRNU) as sensor noise [9], [12] along with model-specific features in the image. Having enough data from multiple devices of each model would have helped the network to generalize further on this task. Therefore, to detect the source camera model effectively, we need to take care that the network does not become dependent on device specific sensor noise. In addition to this, various post-processing operations are generally introduced in the images which alter the spatial structure of the features in an unpredictable manner. Therefore, a network that can detect the model-specific features under all of these constraints needs to be designed and trained in such a way that it excludes the device-specific features as much as possible and is able to focus on the model-specific features.

The design of our proposed remnant block addresses all

TABLE I
ARCHITECTURE OF THE i -TH REMNANT BLOCK

Layers	Output Size	Kernels*
BN	$64 \times 64 \times 3$	–
Conv 2D & BN	$64 \times 64 \times f_i$	$F = f_i, K = 3 \times 3, S = 1$
Concatenate	$64 \times 64 \times (f_i + 3)$	
Conv 2D & BN	$64 \times 64 \times f_i$	$F = f_i, K = 3 \times 3, S = 1$
Concatenate	$64 \times 64 \times (f_i + 3)$	
Conv 2D & BN	$64 \times 64 \times 3$	$F = 3, K = 3 \times 3, S = 1$
Subtract	$64 \times 64 \times 3$	–

* The letters F, K, and S represent the number of filters, their kernel size, and strides, respectively, in the corresponding convolution layers.

the above mentioned issues. The problem of diminishing minute model-specific features is alleviated in the remnant block through the use of skip connections. To preserve input information throughout a block, the input is propagated to every convolutional layer inside the block. Even if some of the minute features are lost in a layer, it is regenerated through the skip connections (see Fig. 3(b)). This also prevents the vanishing of gradient-flow during training. We do not use any activation function in our remnant blocks because we prefer to build the remnant blocks as optimal digital filters that will act as preprocessors for CMI. The final layer of a block is subtracted from the input in a pixelwise fashion. The motivation behind this subtraction operation is to regulate information flow, suppress the contents of an image, and utilize the remnant after the successive convolution operations.

There are several hyperparameter choices in the final structure of our preprocessing scheme: the number of remnant blocks, the depth of a single block, the number of filters in each layer, and kernel size— all of these are set using cross-validation. The architecture of the remnant block is depicted in Table I. Each block consists of 3 convolutional layers with kernel size 3×3 followed by BN. Inside each block, the feature space is widened from $64 \times 64 \times 3$ to $64 \times 64 \times f_i$ in the first 2 convolutional layers and then reduced to $64 \times 64 \times 3$ again in the last convolutional layer. The choice for f_i in the consecutive remnant blocks are 64, 128, and 256, respectively. The output of the final convolutional layer in a block is subtracted from the input. As the convolutional layers are followed by BN, in spite of directly using the input, we use the batch normalized version of it. The contribution of the remnant blocks in RemNet is experimentally verified in our experimental results section (see Table IV).

The remnant blocks are somewhat influenced by the highway networks proposed by Srivastava et al. in [33]. A plain convolutional layer applies a nonlinear transformation H (parameterized by \mathbf{W}_H) on its input \mathbf{x} to produce its output \mathbf{y} :

$$\mathbf{y} = H(\mathbf{x}, \mathbf{W}_H), \quad (10)$$

where H is usually an affine transform followed by a nonlinear activation function, but it may take different forms for different

TABLE II
ARCHITECTURE OF OUR PROPOSED REMNET

Layers	Output Size	Kernels*
Remnant Block 1	$64 \times 64 \times 3$	$f_1 = 64$
Remnant Block 2	$64 \times 64 \times 3$	$f_2 = 128$
Remnant Block 3	$64 \times 64 \times 3$	$f_3 = 256$
Classification Block		
Conv 2D, BN, & PReLU	$32 \times 32 \times 64$	$F = 64, K = 7 \times 7, S = 2$
Conv 2D, BN, & PReLU	$16 \times 16 \times 128$	$F = 128, K = 5 \times 5, S = 2$
Conv 2D, BN, & PReLU	$8 \times 8 \times 256$	$F = 256, K = 3 \times 3, S = 2$
Conv 2D, BN, & PReLU	$4 \times 4 \times 512$	$F = 512, K = 2 \times 2, S = 2$
Average Pool	$1 \times 1 \times 512$	$K = 4 \times 4$
Conv 2D	$1 \times 1 \times 18$	$F = N, K = 1 \times 1, S = 1$
Softmax	N	–

* The letters F, K, and S represent the number of filters, their kernel size, and strides, respectively, in the corresponding convolution layers.

tasks.

For a highway network, two nonlinear transforms $T(\mathbf{x}, \mathbf{W}_T)$ and $C(\mathbf{x}, \mathbf{W}_C)$ are defined such that

$$\mathbf{y} = H(\mathbf{x}, \mathbf{W}_H) \cdot T(\mathbf{x}, \mathbf{W}_T) + \mathbf{x} \cdot C(\mathbf{x}, \mathbf{W}_C), \quad (11)$$

where T is the transform gate and C is the carry gate. T controls how much of the activation is passed through and C controls how much of the unmodified input is passed through. Our remnant blocks are motivated by these two gating units. We make significant modifications in our transformation function H because of the nature of the operation we want to perform. As the remnant blocks are intended to be designed as a linear preprocessor, as stated before, we avoid the use of nonlinear activation functions. Also, we make use of multiple intra-block skip connections in our remnant block to preserve input information throughout a block. We use a pixelwise subtraction operation that regulates the flow of information and alleviates the loss of information through successive convolutional operations. For the above mentioned reasons, our transform and carry gate are linear in nature and we set T and C as -1 and 1 , respectively. In our case, (11) becomes

$$\mathbf{y} = \mathbf{x} - H(\mathbf{x}, \mathbf{W}_H). \quad (12)$$

The residual network (ResNet) [34] is also a variant of the highway network [35] where the choices for both T and C are 1 for the residual blocks. However, the transformation H used in [34] works as a nonlinear feature extractor whereas the H of our remnant blocks performs linear filtering operation. In addition, ResNet does not use any skip connections.

To demonstrate that the dynamically designed remnant blocks truly performs the desired pre-processing task, we show in Fig. 4 the outputs of the final remnant block along with their frequency characteristics for an arbitrarily selected

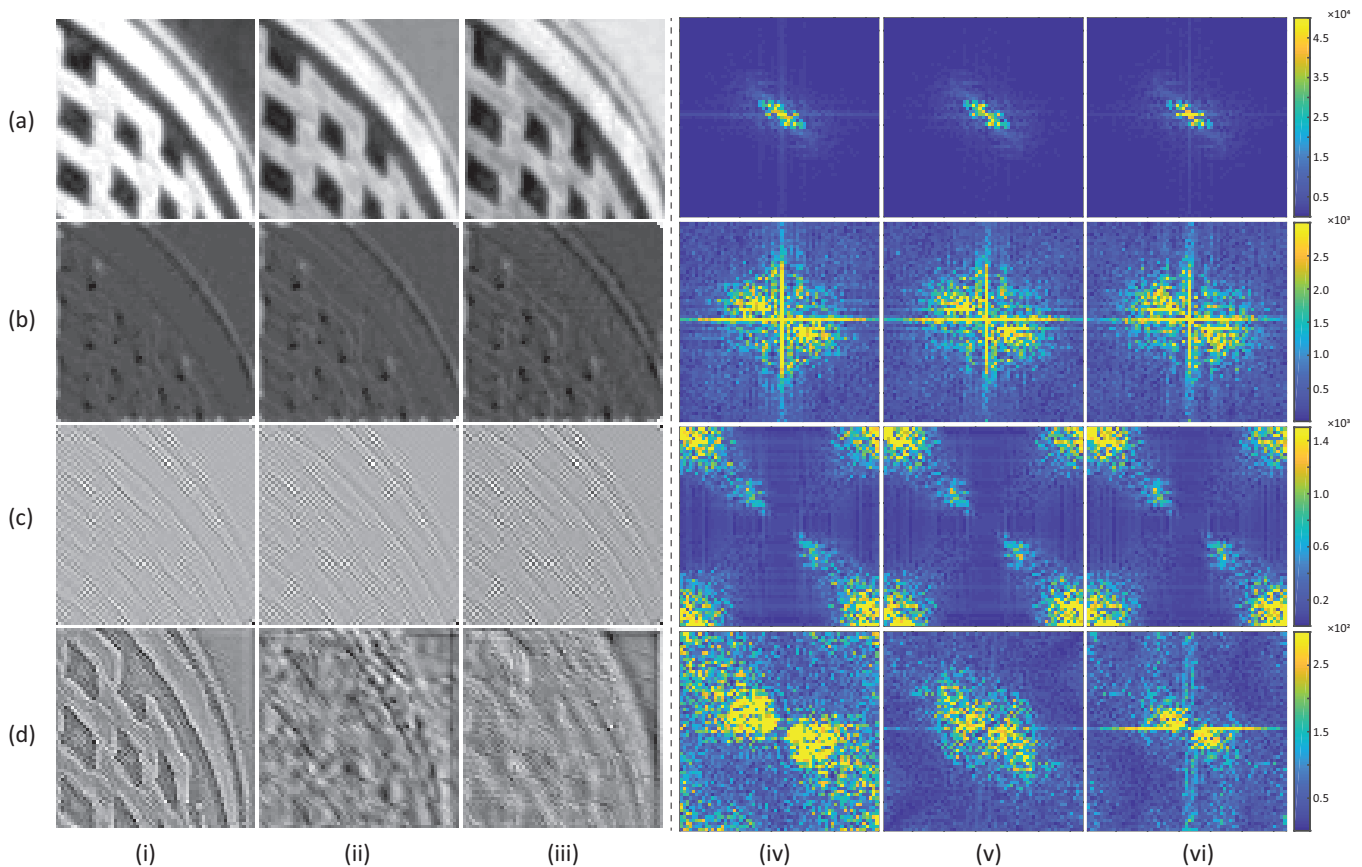


Fig. 4. Comparison of outputs of various pre-processing schemes. (a) Input image, (b) median filter residue, (c) high-pass filter output, and (d) output of the third remnant block of our proposed RemNet. Columns (i), (ii), and (iii) correspond to the three output channels whereas columns (iv), (v), and (vi) depict their frequency responses, respectively.

3-channel image. We also make a spatial and frequency domain comparison of the conventional filters, e.g., median and high-pass filters used in [18], [19], respectively. Fig. 4(a) shows the original 3-channel RGB image, Figs. 4(b)-4(d) show the median filtered residue, high-pass filtered output, and the output of the last remnant block, respectively. If we observe the frequency domain representation of the three output channels of our remnant block, we notice that it is not constrained in the frequency domain. The first channel encompasses information from the full frequency range whereas the other two channels mostly learn distinct low frequency components. On the other hand, the fixed preprocessing performs the same operation on 3 channels and discard information of a certain range of frequencies. We claim that our data adaptive preprocessing performs better filtering operation as it preserves the camera signature from a wide range of frequencies. This claim is supported by Lukas et al. [12] where they have explicitly stated that both low and high frequency information are required for CMI. The distinctive competency of the remnant blocks is experimentally verified in Section IV.

2) *Classification block*: The output of the final remnant block, of size $(64 \times 64 \times 3)$, is passed to another module we name as classification block which is outlined in Table II. The aim of this module is to extract higher level camera

model-specific features, reduce the dimensions of the feature vectors, and eventually generate a class probability of the source camera model of the input image.

The classification block has four consecutive convolution layers at the beginning. Each of the convolutional layer is followed by a BN layer and a PReLU activation. The output of the fourth convolutional layer, of size $(4 \times 4 \times 512)$, is followed by an average-pooling operation which reduces the feature vector to a size of $(1 \times 1 \times 512)$. Finally, we pass the average-pooled feature vector to a final convolution layer with softmax activation to generate probabilities for the N number of camera models.

Instead of using max-pool operation, we use strided convolution to reduce the feature space in the first four convolution layers. This makes the feature reduction process learnable and much less aggressive compared to max-pool [36]. As per the design principles introduced in [20], we gradually decrease the kernel size in the first convolution layers. The BN layer is included for regularization and faster convergence.

Previously CNNs used the ReLU activation function [37]. But here we want to emphasize on extracting camera model fingerprints which are statistical in nature. They do not necessarily have to be positive. As we do not want to put any constraint on the feature generation, we use the PReLU activation function in our classification block. Also when CNNs used with a PReLU activation function, it has exper-

imentally demonstrated higher accuracy [25]. We have also experimentally verified this in our experimental results section (see Table IV).

The average-pool operation is used as per the conventional design structure of CNNs [34], [38], [39] to reduce the dimensionality of the feature space before making the final decision. We do not use fully connected layers in the classification block to keep the number of parameters less which makes the network less prone to overfitting. This also helps the network train faster.

IV. EXPERIMENTAL RESULTS

To demonstrate the effectiveness of our proposed RemNet, we conduct a number of experiments. In this section, we discuss those experimental results in detail. All of the experiments regarding training and implementation of the model are performed in a hardware environment which includes Intel Core-i7 8700K, 3.70 GHz CPUs and Nvidia GeForce GTX 1080 Ti (11 GB Memory) GPU. The necessary codes are written in Python and the neural network models were implemented by using the Keras API (version 2.1.6) with TensorFlow-GPU (version 1.8.0) in the backend.

A. Results on Dresden Dataset

We comprehensively evaluate our model on Dresden Dataset [40]. These images are captured with 73 devices of 25 different camera models. Multiple shots have been taken from several locations (e.g., office, public square, etc.) for each device. Different pictures are acquired from different viewpoints (e.g., looking on the right, on the left, etc.) for each location. The acquisition process is explained in detail in [40]. In our work, we choose only those camera models which have more than one device so that we can keep one device separate for testing purpose. This results in discarding 7 camera models. Of the rest 19 devices, we consider two camera models, Nikon D70 and Nikon D70s, as a single model based on the work of Kirchner et al. [2]. Consequently, we have 18 camera models (see Table III). We use *scene* to refer to combination of a location and a specific viewpoint.

We split the dataset into train, validation, and test sets in such a way that the camera device and scenes used during testing are never used for training or validation. For each camera model, we set one device apart for evaluation. This results in 7938, 1353 and 540 images in the train, validation and test set, respectively (see Table III). This splitting policy, proposed in [41], is of paramount importance so that we can be sure that the neural network does not overfit on the training data and the testing accuracy is not biased by device specific features or the natural contents of the scene.

We extract 256×256 sized clusters of pixels from the original image. However, it is to be noted that all clusters of pixels from an image are not rich in camera model-specific features. In particular, saturated and flat regions are not likely to contain enough statistical information about the camera model. Therefore, after extracting clusters, we determine their quality and only use clusters of good quality to train and test our network. We compute the quality value of a cluster as

TABLE III
CAMERA MODELS OF THE DRESDEN DATABASE USED IN OUR EXPERIMENTS

Model No.	Camera Model	No. of Images	No. of Devices	
			Train and Val.	Test
1	Canon IXUS 70	363	2	1
2	Casio EX-Z150	692	4	1
3	FujiFilm FinePix J50	385	2	1
4	Kodak M1063	1698	4	1
5	Nikon Coolpix S710	695	4	1
6	Nikon D200	373	1	1
7	Nikon D70 Nikon D70S	373	1 1	1 1
8	Olympus μ 1050SW	782	4	1
9	Panasonic DMC-FZ50	564	2	1
10	Pentax Optio A40	405	3	1
11	Praktica DCZ 5.9	766	4	1
12	Ricoh Capilo GX100	559	4	1
13	Rollei RCP-7325XS	377	2	1
14	Samsung L74wide	441	2	1
15	Samsung NV15	412	2	1
16	Sony DSC-H50	253	1	1
17	Sony DSC-T77	492	3	1
18	Sony DSC-W170	201	1	1
	Total	9831		

outlined in [41]. For each cluster \mathcal{P} in an image, its quality $Q(\mathcal{P})$ is computed as

$$Q(\mathcal{P}) = \frac{1}{3} \sum_{c \in [R, G, B]} [\alpha \cdot \beta \cdot (\mu_c - \mu_c^2) + (1 - \alpha) \cdot (1 - e^{-\gamma \sigma_c})] \quad (13)$$

where α , β , and γ are empirically set constants (set to 0.7, 4 and $\ln(0.01)$, respectively), μ_c and σ_c , $c \in [R, G, B]$ are the mean and standard deviation of the red, green, and blue components of cluster \mathcal{P} , respectively. For cluster of pixels with texture, this quality measure tends to be higher than for the overly saturated or flat clusters (see Fig. 5). We found that this quality assessment is consistent with the ‘others’ category mentioned in [21]. According to the definition in [21], 99.32% of our quality clusters fall into *others* category while 0.63% are *smooth* and the rest 0.03% are *saturated*. Therefore, we can consider that our cluster selection strategy is almost identical to choosing the ‘others’ category patches of Yang et al. [21].

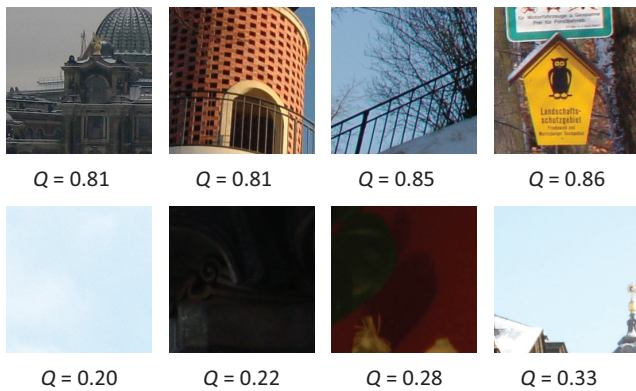
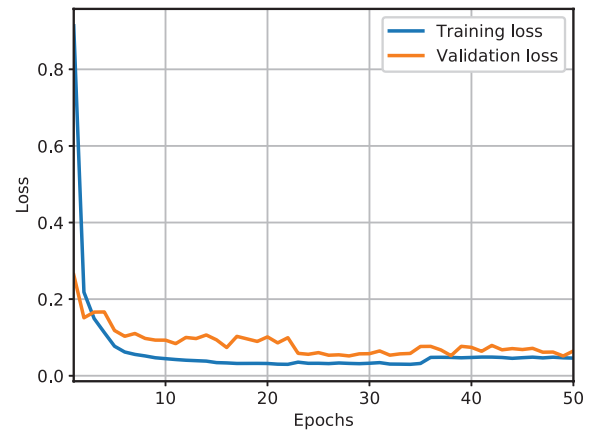


Fig. 5. Examples of clusters of different qualities with their quality indices. The top row represents good quality clusters and the bottom row represents bad quality clusters.

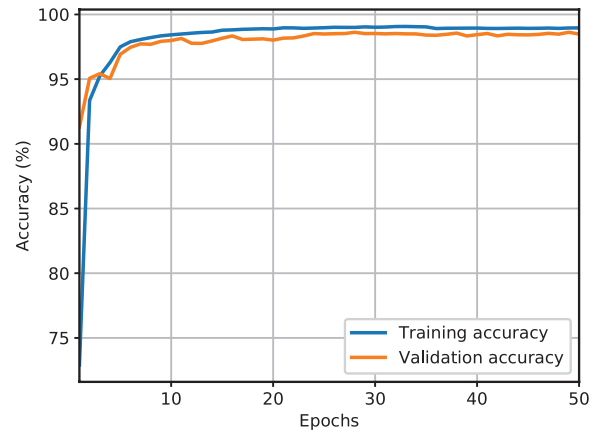
Although we extract 256×256 sized good clusters from the main image, the input patch size that we opt to use for our network is 64×64 as suggested in [21], [41] and [42]. During training, we select a patch of size 64×64 randomly from a cluster of 256×256 in each iteration. The idea of small input patch of 64×64 is motivated by 3 reasons: (i) it results in more data to train our proposed network; (ii) during test, it enables us to generate multiple predictions for a given image and averaging over all of those predictions may ensure a more accurate classification; (iii) training our network with patches of smaller size relative to the image prevents our network from learning dominant spatial features of the image affixed directly to its contents, subsequently enabling the network to learn inherent model-specific statistical features. Also, training a network with bigger input patch size poses hardware constraints and requires more time.

Our cluster selection strategy introduces statistical variations during training. The network cannot rely on seeing the same patch of size 64×64 more than once. This has a regularizing effect and forces the network to learn more robust features that generalizes better across multiple samples of the input data. Our proposed cluster selection method also ensures that the input patches of 64×64 to the network are a mix of good and bad patches where good patches are dominant in number. Some of the good clusters of 256×256 may contain few bad patches of 64×64 (see Fig. 5). Therefore, during training, the network learns to extract features from saturated regions as well. This in turns helps our network to perform well in bad clusters extracted from the main image which is demonstrated in the experimental section.

We extract 20 clusters of size 256×256 from each image and this results in 158760 and 27060 clusters for the train and validation set. During training, we randomly crop a 64×64 size patch from each cluster in each epoch and feed it to the network. We use categorical cross-entropy as the loss function and Adam [31] as the optimizer with the exponential decay rate factors $\beta_1 = 0.9$ and $\beta_2 = 0.999$. The batch size we opt to use is 64. The initial learning rate is set to 10^{-3} and is decreased by a factor of 0.5 if the validation loss does not decrease in two successive epochs. When the learning rate is reduced to 10^{-7} , the training is stopped. In this way,



(a)



(b)

Fig. 6. Training history of our proposed RemNet. (a) Loss vs. epochs and (b) accuracy vs. epochs.

we train our network for a maximum of 50 epochs and save the weight with the least validation loss for evaluation. The corresponding training history is shown in Fig. 6. It shows that our model quickly converges at around 20-30 epochs. The validation loss decreases gradually with the training loss and there is no significant gap between them. This indicates that our network does not tend to overfit.

After training, we test our network on the testing set comprised of 18 different camera models of the Dresden database. The test set contains 10800 clusters of size 256×256 from 540 full images, which all are from a separate device and *scene* that is unseen to the network during the training stage. During testing, we select N number of clusters of size 256×256 from a test image according to our quality assessment. To make prediction for each 256×256 cluster, we take the average of the predictions on all non-overlapping patches of size 64×64 it contains and assign a camera model label \hat{L}_n to it. The final prediction \hat{L} for the entire image is obtained through majority voting on \hat{L}_n for $n \in [1, N]$.

First, we experiment with several design choices of RemNet. We train and test these various designs on the Dresden dataset. The results of these experiments are presented in Table IV.

TABLE IV
ACCURACY (IN %) FOR DIFFERENT DESIGN CHOICES OF REMNET ON THE TEST SET OF DRESDEN DATASET

Design Choice	Accuracy
Remnant Blocks + Classifier (ReLU)	96.48
Remnant Blocks + Classifier (PReLU)	97.03
Remnant Blocks with Activation (PReLU) + Classifier (PReLU)	96.67
Only Classifier (PReLU)	93.33

It is evident from this table that our proposed RemNet with 3 remnant blocks followed by a classification block with PReLU activation results in a better accuracy. Using only the classifier block to identify camera models directly from the images results in the worst performance which proves that a preprocessing block is indeed necessary for CMI.

For CMI, the detection accuracy of RemNet is 97.03% for $N = 20$. We compare our results with two established networks— constrained-convolutional network [20] and fusion residual network [21]. Since, we use good quality cluster of pixels that is in commensurate with the ‘others’ category [21], we do not implement the fusion residual network for three different categories mentioned in the respective paper. For fair comparison, we use the same input patch size, 64×64 , for all the networks. The implementation of each method is made under careful scrutiny. The results presented in Table V shows that our proposed architecture performs better than those in [20], [21].

Our goal has been to design a robust network that can perform CMI even if the image is post-processed. To address this challenge, we train the networks by augmenting the training and validation sets so as to make the networks familiar with manipulated images. The types of augmentation that have been performed are:

- JPEG-Compression with quality factor of 70%, 80%, and 90%
- Resizing by a factor of 0.5, 0.8, 1.5, and 2.0
- Gamma-Correction using $\gamma = 0.8$ and 1.2

This increases our train and validation data 9 fold resulting in 1587600 and 270600 train and validation clusters, respectively. After training on this augmented dataset, evaluation is carried out on the test set. From Table V, it is evident that, our proposed RemNet performs substantially better than the other two methods with an accuracy of 97.59%. It is worthwhile to mention that our model attains 100% accuracy on identifying 16 camera models. For the rest of the two camera models,

TABLE V
ACCURACY (IN %) OF DIFFERENT METHODS ON DRESDEN DATASET

Method	Dresden Dataset	
	Unaltered	Augmented
Yang et al. [21]	94.81	95.19
Bayar et al. [20]	95.56	93.89
Proposed RemNet	97.03	97.59

Sony DSC-H50 and Sony DSC-W170, attain accuracy of 90% and 75%, respectively. The decrease in the identification accuracy of these two exact models has also been observed in [19]. As mentioned in [2], images captured with camera models of the same manufacturer are likely to share some components which makes it harder to separate them.

In Fig. 7, we observe the effect of voting number on the performance of different networks. For the good clusters (see Fig. 7(a)), our network shows a somewhat steady trend whereas the other two networks show oscillatory behavior. This proves that the performance our network is nearly independent of the voting number of clusters. However, an optimum voting number has to be selected for the other two networks. On the other hand, for prediction on bad clusters of an image, the accuracy gradually increases with the increment of voting number for all three networks as is evident from Fig. 7(b). In both of these two cases our proposed RemNet outperforms the networks (i.e., [20] and [21]) in comparison.

In order to verify the robustness of the networks trained with the augmented dataset, we apply various post-processing operations on the test set and evaluate their performance. To further ensure that the network is not biased toward the train set, we perform post-processing on test images with such

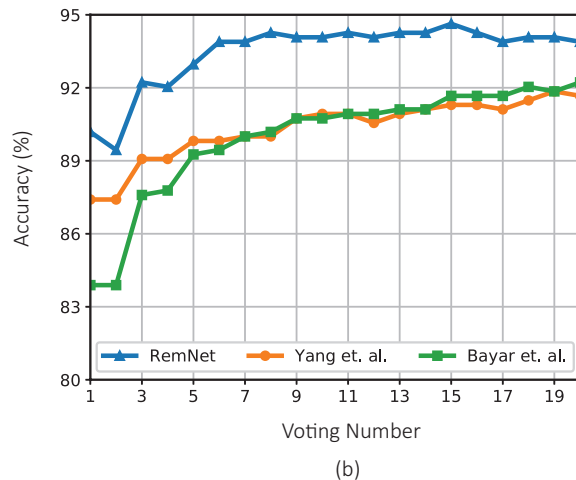
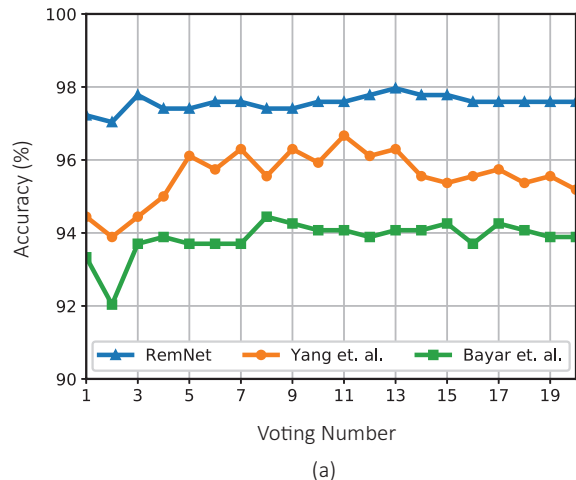


Fig. 7. Results of varying voting number for (a) good clusters and (b) bad clusters.

TABLE VI
COMPARATIVE RESULTS OF OUR PROPOSED REMNET WITH DIFFERENT METHODS IN IDENTIFYING CAMERA MODELS FROM MANIPULATED IMAGES (ACCURACY IN %)

Manipulation Factor	Gamma Correction				JPEG Compression				Resize Scale			
	0.5	0.75	1.25	1.5	95	90	85	80	0.8	0.9	1.1	1.2
Yang et al. [21]	94.26	95.37	95.00	92.78	94.07	94.07	92.59	92.59	94.26	92.59	90.93	90.56
Bayar et al. [20]	93.52	94.44	94.44	94.63	92.59	94.81	88.15	85.74	88.15	87.04	64.44	59.07
RemNet	96.11	97.22	96.11	95.56	97.59	94.81	92.59	92.78	95.00	93.33	92.04	92.41

factors that are not necessarily used in the augmented train and validation set. We process the images using gamma correction with $\gamma = 0.5, 0.75, 1.25, \text{ and } 1.5$; JPEG compression quality factors (QFs) 95%, 90%, 85%, and 80%; and resize scaling factor of 0.8, 0.9, 1.1, 1.2. In all the subsequent experiments, we apply the post-processing operation directly on the original test set images and then extract clusters as mentioned before. The results are presented in Table VI. In all the experiments, our proposed RemNet outperforms the other networks with a significant margin which proves that RemNet has the potential to identify camera models in real world scenarios. Of the other two networks, the network proposed by Yang et al. [21] performs considerably better than the network proposed by Bayar et al. [20] in JPEG compression and rescaling. In [12], it is mentioned that gamma correction has little influence on the reliability of camera model identification. Our experimental results (see Table VI) show similar behavior for all the three networks with an exception for [21] at gamma correction factor of 1.5.

B. Results on SP-Cup Dataset

To test the generalizability of our approach, we have also trained and tested the network on the CMI Dataset provided for the IEEE Signal Processing (SP) Cup 2018. The training dataset provided by the IEEE Signal Processing Society consists of images captured by 10 different camera models having 275 images for each model. Since, only one device is used to capture these images for each camera model, we collect external data from multiple devices from Flickr under the creative commons license. All these images are used for training and validation purposes only. A brief summary of the dataset is given in Table VII.

The dataset described in Table VII is split into train and validation data by 3:1 ratio. The test dataset is provided separately which includes 2640 images of size 512×512 , among which 1320 are unaltered and the rest are augmented, i.e., resized, gamma corrected or JPEG compressed. All the test images are acquired with a separate device other than the ones used for capturing training images.

The training and testing is done by following the same procedures as mentioned in the earlier experiments. This time, we train our network for 10 classes. The testing is done on the test set which are images from completely separate devices that are used for training. Since the size of the test images is 512×512 , we extract the best cluster of size 256×256 and generate result following the testing procedure mentioned previously. According to the competition rules of

TABLE VII
SP CUP DATA AND FLICKR DATA

Camera Model	SP Cup Data (No. of Images)	Flickr Data (No. of Images)
HTC-1-M7	275	746
iPhone-4s		499
iPhone-6		548
LG-Nexus-5x		405
Motorola-Droid-Maxx		549
Motorola-Nexus-6		650
Motorola-X		344
Samsung-Galaxy-Note3		274
Samsung-Galaxy-S4		1137
Sony-NEX-7		557
Sub-Total	2750	5709
Grand-Total	8459	

IEEE Signal Processing Cup 2018, the score on the test-results are calculated based on the following formula:

$$\text{Score} = 0.7 \times (\text{Accuracy of Unaltered Images}) + 0.3 \times (\text{Accuracy of Manipulated Images}). \quad (14)$$

From Table VIII, we can clearly see that our proposed RemNet outperforms the other established methods with an accuracy of 95.11%. This satisfactory performance is an evidence of the generalizability of our proposed RemNet. The bad performance of [20] may be attributed to the shallowness of the network. The training data consists of Flickr images that may have gone through different kinds of post-processing with the help of image editing tools, e.g., Adobe Photoshop and Adobe Lightroom. We can hypothesize that the extraction of camera model-specific features from these extensively post-processed images would require a deeper network.

TABLE VIII
ACCURACY (IN %) OF DIFFERENT METHODS ON SP CUP TESTING DATASET

Yang et al. [21]	Bayar et al. [20]	RemNet
94.83	90.97	95.11

TABLE IX
RESULTS ON IMAGE MANIPULATION DETECTION FOR DIFFERENT MANIPULATION FACTORS (ACCURACY IN %)

Manipulation Factor	Gamma Correction				JPEG Compression				Rescale			
	0.5	0.75	1.25	1.5	95	90	85	80	0.8	0.9	1.1	1.2
Yang et al. [21]	99.07	98.52	97.04	98.70	49.44	100	100	100	100	97.40	60.74	100
Bayar et al. [20]	94.44	83.33	77.22	90.56	11.30	100	100	100	100	100	90.93	99.63
RemNet	100	99.81	99.63	100	81.48	98.33	100	100	100	100	100	100

C. Image Manipulation Detection

Now, we show the use of our network in a completely different image forensic task. We use it to identify the kind of image-manipulation done on an image. The same network architecture is used here except the number of output classes, which in this case is 4 – unaltered, rescale, JPEG compression, and gamma correction. The input patch size for all the networks is also maintained at (64×64) . We use the same augmented train and validation set from our experiments with Dresden dataset and sub-divided it into the 4 manipulation classes. RemNet is then trained to detect the type of manipulation applied to an image. It is to be mentioned that, during training, our dataset consisting of 1587600 train and 270600 validation clusters has been reduced in order to make the training data evenly distributed among 4 classes. Since the number of unaltered train and validation clusters are 158760 and 27060, respectively, we select 158760 train and 27060 validation clusters randomly for each type of manipulation.

In testing, we have used the test images from the Dresden dataset and generated a total of $540 \times 13 = 7020$ test images, which include 540 unaltered images; $540 \times 4 = 2160$ gamma corrected images with $\gamma = 0.5, 0.75, 1.25, \text{ and } 1.5$; $540 \times 4 = 2160$ JPEG compressed images with factors of 80%, 85%, 90%, and 95%; and $540 \times 4 = 2160$ resized images with scaling factor of 0.8, 0.9, 1.1, and 1.2. Details of the results are given in Table IX. We achieve an overall accuracy of 98.27% in this task whereas [20] and [21] achieve 87.28% and 91.74%, respectively. We demonstrate the detection accuracy for different factors of manipulation in Table IX. For gamma corrected images, the performance of RemNet is the best whereas [21] performs substantially better than [20]. In case of JPEG compression factors of 90%, 85% and 80%, all three networks perform the same except the slight decrease in accuracy for RemNet at the factor of 90%. However, at the compression factor of 95%, [20] and [21] fail miserably by misclassifying most of the compressed images as unaltered images. This is expected since there is very little difference between the original image and JPEG compressed image with a compression factor of 95. The considerably better detection accuracy of RemNet for this compression factor proves its ability to detect subtle changes in an image. When detecting rescaled images, our network performs the best by attaining a 100% accuracy. Of the other two networks, [20] performs better than [21].

The ability of the remnant blocks to perform different kinds of preprocessing as needed becomes evident if we compare Fig. 4(d(i-iii)) and Fig. 8. Comparing these outputs generated

for the same input image, we can conclude that the remnant block is able to perform task specific preprocessing. Therefore, we can hypothesize that different types of preprocessing would be necessary for different image forensic tasks.

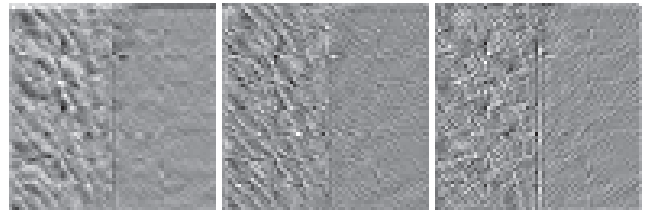


Fig. 8. Output of the last remnant block as obtained for manipulation detection.

V. CONCLUSION

In this paper, we have proposed a novel CNN based architecture called RemNet for identifying the source camera-model of an image. RemNet comprises of multiple remnant blocks with intra-block skip connections and a classification block in series. Unlike the conventional fixed filters used for preprocessing in image forensics, our proposed novel remnant blocks are completely data driven. It suppresses unnecessary image contents dynamically and generates a remnant of the image from where the classification block can easily extract intrinsic camera model-specific features. We have comprehensively conducted multiple experiments on Dresden dataset to demonstrate the efficacy of RemNet in CMI. The results of the experiments have shown that RemNet can be successfully used in real-world scenarios. The performance on IEEE Signal Processing Cup 2018 Camera Model Identification dataset has proven further the generalizability of our network. Additionally, we have used RemNet for image manipulation detection. The satisfactory performance of our network on this task indicates that it can be used as a general purpose network for different image forensic tasks. We wish to further extend our work in the future to explore the potentiality of RemNet in other image forensic tasks such as forgery detection.

REFERENCES

- [1] M. C. Stamm, M. Wu, and K. R. Liu, "Information forensics: An overview of the first decade," *IEEE Access*, vol. 1, pp. 167–200, 2013.
- [2] M. Kirchner and T. Gloe, "Forensic camera model identification," *Proc. WOL Handbook of Digital Forensics of Multimedia Data and Devices*, pp. 329–374, 2015.
- [3] A. Piva, "An overview on image forensics," *Proc. ISRN Signal Process.*, vol. 2013, 2013.
- [4] H. Farid, "Image forgery detection," *IEEE Signal Process. Mag.*, vol. 26, no. 2, pp. 16–25, 2009.

- [5] S. Bayram, H. Sencar, N. Memon, and I. Avcibas, "Source camera identification based on cfa interpolation," in *Proc. IEEE Int. Conf. on Image Process., (ICIP)*, vol. 3, 2005, pp. III–69.
- [6] M. Kharrazi, H. T. Sencar, and N. Memon, "Blind source camera identification," in *Proc. IEEE Int. Conf. on Image Process., (ICIP)*, vol. 1, 2004, pp. 709–712.
- [7] T. Gloe, "Feature-based forensic camera model identification," in *Transactions on Data Hiding and Multimedia Secur. VIII*. Springer, 2012, pp. 42–62.
- [8] A. E. Dirik, H. T. Sencar, and N. Memon, "Source camera identification based on sensor dust characteristics," in *Proc. IEEE Applications for Public Secur. and Forensics in Signal Process.*, 2007, pp. 1–6.
- [9] J. Fridrich, J. Lukas, and M. Goljan, "Digital camera identification from sensor noise," *IEEE Trans. Inf. Forensics Security*, vol. 1, no. 2, pp. 205–214, 2006.
- [10] T. Filler, J. Fridrich, and M. Goljan, "Using sensor pattern noise for camera model identification," in *Proc. IEEE ICIP 2008. 15th IEEE Int. Conf. on Image Process.*, 2008, pp. 1296–1299.
- [11] T. H. Thai, R. Cogranne, and F. Retraint, "Camera model identification based on the heteroscedastic noise model," *IEEE Trans. Image Process.*, vol. 23, no. 1, pp. 250–263, 2014.
- [12] J. Lukas, J. Fridrich, and M. Goljan, "Digital camera identification from sensor pattern noise," *IEEE Trans. Inf. Forensics Security*, vol. 1, no. 2, pp. 205–214, 2006.
- [13] H. Cao and A. C. Kot, "Accurate detection of demosaicing regularity for digital image forensics," *IEEE Trans. Inf. Forensics Security*, vol. 4, no. 4, pp. 899–910, 2009.
- [14] A. Swaminathan, M. Wu, and K. R. Liu, "Nonintrusive component forensics of visual sensors using output images," *IEEE Trans. Inf. Forensics Security*, vol. 2, no. 1, pp. 91–106, 2007.
- [15] C. Chen and M. C. Stamm, "Camera model identification framework using an ensemble of demosaicing features," in *Proc. IEEE Int. Workshop on Inf. Forensics and Secur. (WIFS)*, 2015, pp. 1–6.
- [16] F. Marra, G. Poggi, C. Sansone, and L. Verdoliva, "A study of co-occurrence based local features for camera model identification," *Multimedia Tools and Applications*, vol. 76, no. 4, pp. 4765–4781, 2017.
- [17] J. Schmidhuber, "Deep learning in neural networks: An overview," *Neural networks*, vol. 61, pp. 85–117, 2015.
- [18] J. Chen, X. Kang, Y. Liu, and Z. J. Wang, "Median filtering forensics based on convolutional neural networks," *IEEE Signal Process. Lett.*, vol. 22, no. 11, pp. 1849–1853, 2015.
- [19] A. Tuama, F. Comby, and M. Chaumont, "Camera model identification with the use of deep convolutional neural networks," in *Proc. IEEE Int. Workshop on Inf. Forensics and Secur. (WIFS)*, 2016, pp. 1–6.
- [20] B. Bayar and M. C. Stamm, "Design principles of convolutional neural networks for multimedia forensics," *Electronic Imaging*, vol. 2017, no. 7, pp. 77–86, 2017.
- [21] P. Yang, W. Zhao, R. Ni, and Y. Zhao, "Source camera identification based on content-adaptive fusion network," *arXiv preprint arXiv:1703.04856*, 2017.
- [22] B. Li, Y. Q. Shi, and J. Huang, "Detecting doubly compressed jpeg images by using mode based first digit features," in *Proc. IEEE 10th Workshop on Multimedia Signal Process.*, 2008, pp. 730–735.
- [23] M. C. Stamm and K. R. Liu, "Forensic detection of image manipulation using statistical intrinsic fingerprints," *IEEE Trans. Inf. Forensics Security*, vol. 5, no. 3, pp. 492–506, 2010.
- [24] E. Kee, M. K. Johnson, and H. Farid, "Digital image authentication from jpeg headers," *IEEE Trans. Inf. Forensics Security*, vol. 6, no. 3, pp. 1066–1075, 2011.
- [25] B. Bayar and M. C. Stamm, "A deep learning approach to universal image manipulation detection using a new convolutional layer," in *Proc. 4th-ACM Workshop on Inf. Hiding and Multimedia Secur.*, 2016, pp. 5–10.
- [26] Y. LeCun, Y. Bengio, and G. Hinton, "Deep learning," *nature*, vol. 521, no. 7553, p. 436, 2015.
- [27] V. Nair and G. E. Hinton, "Rectified linear units improve restricted boltzmann machines," in *Proc. of the 27th Int. Conf. on machine learning (ICML-10)*, 2010, pp. 807–814.
- [28] K. He, X. Zhang, S. Ren, and J. Sun, "Delving deep into rectifiers: Surpassing human-level performance on imagenet classification," in *Proc. IEEE Int. Conf. Comput. Vis.*, 2015, pp. 1026–1034.
- [29] S. Ioffe and C. Szegedy, "Batch normalization: Accelerating deep network training by reducing internal covariate shift," *arXiv preprint arXiv:1502.03167*, 2015.
- [30] H. Robbins and S. Monro, "A stochastic approximation method," in *Herbert Robbins Selected Papers*. Springer, 1985, pp. 102–109.
- [31] D. P. Kingma and J. Ba, "Adam: A method for stochastic optimization," *arXiv preprint arXiv:1412.6980*, 2014.
- [32] M. Chen, J. Fridrich, M. Goljan, and J. Lukás, "Determining image origin and integrity using sensor noise," *IEEE Trans. Inf. Forensics Security*, vol. 3, no. 1, pp. 74–90, 2008.
- [33] R. K. Srivastava, K. Greff, and J. Schmidhuber, "Highway networks," *arXiv preprint arXiv:1505.00387*, 2015.
- [34] K. He, X. Zhang, S. Ren, and J. Sun, "Deep residual learning for image recognition," in *Proceedings of the IEEE Conf. on computer vision and pattern recognition*, 2016, pp. 770–778.
- [35] K. Greff, R. K. Srivastava, and J. Schmidhuber, "Highway and residual networks learn unrolled iterative estimation," *arXiv preprint arXiv:1612.07771*, 2016.
- [36] J. T. Springenberg, A. Dosovitskiy, T. Brox, and M. Riedmiller, "Striving for simplicity: The all convolutional net," *arXiv preprint arXiv:1412.6806*, 2014.
- [37] A. Krizhevsky, I. Sutskever, and G. E. Hinton, "Imagenet classification with deep convolutional neural networks," in *Adv. in neural inf. Process. systems*, 2012, pp. 1097–1105.
- [38] K. Simonyan and A. Zisserman, "Very deep convolutional networks for large-scale image recognition," *arXiv preprint arXiv:1409.1556*, 2014.
- [39] G. Huang, Z. Liu, K. Q. Weinberger, and L. van der Maaten, "Densely connected convolutional networks," in *Proc. of the IEEE Conf. on computer vision and pattern recognition*, vol. 1, no. 2, 2017, p. 3.
- [40] T. Gloe and R. Böhme, "The dresden image database for benchmarking digital image forensics," *J. Digital Forensic Practice*, vol. 3, pp. 150–159, 01 2010.
- [41] L. Bondi, L. Baroffio, D. Güera, P. Bestagini, E. J. Delp, and S. Tubaro, "First steps toward camera model identification with convolutional neural networks," *IEEE Signal Process. Lett.*, vol. 24, no. 3, pp. 259–263, 2017.
- [42] H. Yao, T. Qiao, M. Xu, and N. Zheng, "Robust multi-classifier for camera model identification based on convolution neural network," *IEEE Access*, vol. 6, pp. 24973–24982, 2018.